Original Article

Monte Carlo Simulation of Gamma and Neutron Shielding with High-performance Ultra-heavy Cement Composite

Mohammadreza Alipoor, Mahdi Eshghi, Ramazan Sever[1]

Department of Physics, Imam Hossein Comprehensive University, Tehran, Iran, [1]Department of Physics, Middle East Technical University, Ankara, Turkey

Abstract

Purpose: As the applications of nuclear technology increase in today's world, radiation protection becomes even more important. Radiation protection is important in medical imaging applications and radiotherapy rooms. Therefore, in this research, we have investigated features of the ionizing radiation shielding of the modified cement composite with iron, strontium, zinc, and zirconium elements in the photon energy range of 15 keV to 10 MeV. **Materials and Methods:** To extract such features, it is necessary to use a computational method. In this research, we have done all our calculations based on the Geant4 tool based on the Monte Carlo method. This tool is a multipurpose tool that can be used for particle transport calculations such as electrons, protons, neutrons, heavy charged particles, and photons in different environments such as human tissues. **Results:** The mass attenuation coefficient of the samples was calculated using the Geant4 Monte Carlo simulation tool and compared with the results of the Phy-X program, which was in good agreement. To evaluate the radiation shielding capabilities, other quantities such as the linear attenuation coefficient, the thickness of the tenth value layer, the thermal neutron cross-section, absorption rate of thermal neutrons, and the cross-section of the fast neutron removal are determined. **Conclusions:** According to the quantitative results, cement composite is more effective in absorbing and weakening gamma and neutrons. Calculations of radiation shielding quantities show that cement composites containing tungsten carbide and thallium oxide waste powder are a suitable combination and a practical material for radiation control. In addition, by returning industrial waste to the production sector, they will also be effective in reducing environmental pollution. In general, the cement composite sample containing iron, thallium, zinc, zirconium, tungsten, and carbon elements shows a high potential for radiation protection applications. This study highlights the effective radiation shielding potential of cementitious composites and demonstrates the importance of advancing safety measures in medical and industrial radiation applications.

Keywords: Attenuation coefficient, cements, gamma-ray, Monte Carlo simulations, shielding

Received on: 30-05-2024 **Review completed on: 10-10-2024** **Accepted on: 17-10-2024** **Published on: 18-12-2024**

Introduction

In contemporary times, the burgeoning utilization of radioactive isotopes across various domains, including nuclear energy facilities, radiotherapeutic practices, and industrial applications, has engendered a heightened interest among scholars in the advancement of superior radiation shielding materials. These materials aim to safeguard humans, facilities, and the environment from radiation exposure and the detrimental consequences of neutral radiations such as gamma rays and neutrons. Generally speaking, radiation shielding entails the strategic placement of a material between the radioactive source and individuals or the surrounding environment to mitigate exposure to harmful radiations.[1,2] Gamma and X-ray radiation is most effectively attenuated by dense substances composed of various heavy metals, including lead, nickel, iron, bismuth, barium, and tungsten.[3,4] Conversely, materials that consist of elements with lower atomic numbers, such as carbon, hydrogen, oxygen, and nitrogen, are more suitable for the mitigation of neutron radiation.[5,6] One of the chemical substances that can encapsulate and amalgamate all the previously mentioned elements, which may include aggregates, cement, and water, is indeed a composite material referred to as concrete. The versatility and suitability of concrete can be ascribed to its inherent physical, thermal, mechanical, and other robust

Access this article online

Quick Response Code:

Website: www.jmp.org.in

DOI: 10.4103/jmp.jmp_91_24

Address for correspondence: Dr. Mahdi Eshghi, Department of Physics, Imam Hossein Comprehensive University, Tehran, Iran.
E-mail: eshgi54@gmail.com, meshghi@ihu.ac.ir.

How to cite this article: Alipoor M, Eshghi M, Sever R. Monte Carlo simulation of gamma and neutron shielding with high-performance ultra-heavy cement composite. J Med Phys 2024;49:661-72.

properties. Through the integration of various additives, concrete can be formulated to attain remarkable strength and durability.[7] Furthermore, concrete presents a cost-effective option as a construction material when juxtaposed with other critical building substances such as iron and steel.[8] Nevertheless, despite its extensive acceptance and practical applications, there exist certain environmental and economic concerns associated with its production.[9,10] Initially, concrete is a composite primarily consisting of aggregates and cement. The extraction of aggregates and the quarrying of limestone for the production of concrete and cement, respectively, have been recognized as sources of ecological issues such as soil erosion and flooding. Furthermore, the manufacturing of cement is associated with the release of carbon dioxide, a significant greenhouse gas, thereby substantially contributing to the phenomenon of global warming. In addition, cement production results in the emission of various hazardous gases and particulate matter into the atmosphere.[11,12] Ultimately, the process of cement manufacturing is financially burdensome, necessitating substantial energy consumption. To alleviate the greenhouse gas emissions, costs, environmental degradation, and pollution linked to the procurement of raw materials and the fabrication of cement and concrete, alternative materials may be employed to either partially or wholly supplant concrete or any of its components in civil engineering applications. Numerous alternatives currently available often fail to deliver the structural integrity, longevity, and economic benefits inherent in concrete.[13-16] As a result, the most effective approach to sustain concrete usage while mitigating the economic and ecological ramifications of concrete production has been to partially substitute cement and aggregates in concrete formulation without compromising its mechanical integrity and durability. Cement is regarded as one of the most crucial and expensive constituents in concrete production. Moreover, its manufacturing inflicts a greater degree of environmental harm and pollution when compared to aggregates.[17] The attenuation characteristics of concrete, when mixed with both natural and synthetic particulates, have been explored by numerous researchers. A variety of aggregates, including igneous stones,[18] cement-soil mixtures,[19] basalt,[20] natural minerals,[21] azimuthal materials,[22] and Portland cement,[23] have been incorporated into concrete to augment its gamma radiation shielding efficacy. A considerable number of investigations have been directed toward elevating the attenuation coefficient of concrete for neutron radiation through the incorporation of diverse additives such as boric compounds[24,25] and geopolymers.[26,27] The use of the aforementioned by-products represents an interesting approach due to their low cost and high availability, as well as the fact that the amount of waste produced can meet the needs of the concrete industry. Heavy-weight powder materials can be used as additives to increase the density of cement slurry.[28] Iron ore powders (ilmenite, hematite, and magnetite) are successfully combined as cement-strengthening agents due to their high density and low water requirement. Ramadan *et al*. have reported that the incorporation of ilmenite or hematite barely affects the rheological properties of cement slurry, whereas an even lower water requirement is observed for magnetite powder.[29] Another way to utilize waste metallic powders and tailings is to incorporate them into concretes. Jahan *et al*. have reported the successful incorporation of inorganic fillers in the fabrication and development of modified composites that are used in potential low-energy radiation shielding applications.[30] Similar findings were reported by al-Saleh, where partial replacement of cement with iron filings and bismuth oxide helped to increase the shielding performance of gamma and neutron radiation.[31] In addition to varying mechanical properties, the incorporation of high-density aggregates and powders into cementitious composites has attracted considerable attention for the production of radiation shields against ionizing radiation used in hospitals and commercial radiotherapy.[32] Therefore, extensive efforts are underway to replace lead-based materials with environmentally friendly materials, such as iron ore waste and by-products of mining and crushing processes.[33,34] The Tungsten carbide, a compound known for its remarkable hardness and durability, has furthermore found extensive application in the production of superior-grade cement. Thereby significantly improving and enhancing various essential properties such as strength, wear resistance, and longevity of the cement, which collectively contribute to the overall performance and reliability of the materials used in construction and industrial applications.[35] Thallium is an associated element found in several sulfide and metallic minerals; it is also a byproduct of the smelting and mining sectors, coal-fired power facilities, and the cement manufacturing industry, all of which significantly contribute to soil contamination with this element. Currently, reintegrating this waste into the cement production process not only mitigates environmental impacts but also results in the creation of cement that exhibits resistance to radiation.[36] The implementation of industrial waste as a type of reinforcement in cementitious composites shows considerable promise in the emerging field of recycled materials specifically designed for construction applications and is an innovative approach to achieve a safe and biodegradable shield. It accentuates the environment less. When these optimized recycled composites are subjected to rigorous testing, they demonstrate performance criteria that are not only acceptable but superior to conventionally produced cementitious products, thereby supporting their use as alternatives to traditional concrete mixes.[37-40] In addition, the presence of noncommercial industrial waste materials, which are often underutilized, strengthens the possibility of their integration into sustainable production practices for different building components, thus aligning with environmental protection efforts. Significantly, the lower levels of alkalinity associated with these alternative industrial waste materials, especially when compared to standard commercial Portland cement, may provide significant advantages regarding the durability and long-term performance of cement products reinforced with such industrial by-products. be This innovative approach not only highlights the material properties of cement composites as radiation shields but also

contributes to the overall goal of reducing environmental impacts through the use of industrial waste.

Materials and Methods

This study included the investigation of five types of common building materials and a cement composite, which were different in terms of composition. Types of construction materials examined include Bricks, Concrete, Cement Composites and Spot2, Spot1, and Cement-Plaster. The specific chemical composition of this innovative cement composite that is the subject of our analysis is comprehensively presented in Table 1, which provides crucial insights into its elemental and molecular makeup. In the context of this research endeavor, we shall meticulously evaluate the efficacy of this newly developed cement composite as a viable protective material against the deleterious effects of ionizing radiation, whereas also undertaking a comparative analysis with a variety of other conventional building materials that are commonly.

Theory

In this segment, we succinctly elucidate the theoretical frameworks employed to ascertain the linear attenuation coefficient μ, mass attenuation coefficient μm, half-value layer (HVL), tenth value layer (TVL), and build factor. The linear attenuation coefficient (μ) serves as a pivotal parameter for assessing the impact of gamma rays on the materials under investigation and can be derived from the Beer–Lambert law[41] as demonstrated in equation (1):

$$\mu = \frac{\ln(\frac{I_0}{I})}{x} \tag{1}$$

where I and I_0 denote the photon intensities recorded, and x represents the thickness of the irradiated substance. The mass attenuation coefficient (μ_ρ, cm^2/g) is derived from relation 2 by taking the ratio of μ to the specific weight of the material:[41]

$$\mu_m = \sum_{i=1} W_i (\frac{\mu}{\rho})_i \tag{2}$$

The HVL and the TVL are defined as the specific thicknesses of a given shielding material that are required to attenuate the intensity of incident radiation to half and one-tenth of its original value, respectively; furthermore, the quantitative determination of these crucial parameters can be effectively achieved by employing the mathematical formulations articulated in equations 3 and 4 as referenced in the literature source.[41]

$$HVL(cm) = \frac{ln\,2}{\mu} = \frac{0.693}{\mu} \tag{3}$$

$$TVL(cm) = \frac{ln\,10}{\mu} = \frac{2.3026}{\mu} \tag{4}$$

The quantification of the parameters associated with the effective atomic number, denoted as Z_{eff}, along with the effective electron density, represented as N_{eff}, pertaining to the materials that have been the subject of systematic investigation, is meticulously established through the application of equations numbered five and six as referenced in the scholarly work denoted by the citation.[41]

$$Z_{eff} = \frac{\sum_i n_i A_i (\frac{\mu}{\rho})_i}{\sum_i n_i \frac{A_i}{Z_i} (\frac{\mu}{\rho})_i} \tag{6}$$

$$N_{eff}\left(electron/g\right) = N_A \frac{nZ_{eff}}{A_i}$$

where Z_i atomic number, $N_A = 6.022 \times 10^{23}\ ^1/\text{mol}$, A_i is the atomic weight of ith element.

The quantification of the relative deviation, which is denoted as RD, between the computational outcomes obtained through the Geant4 simulation tool and the theoretical calculations data that has been sourced from the Phy-x database is meticulously determined by employing the mathematical formulation presented in equation 10 as referenced in scholarly work.[41]

$$RD\% = \left|((1-\left(\frac{\mu_{Geant4}}{\mu_{Phy\text{-}x}}\right))\times 100)\right| \tag{7}$$

In the following, the parameters derived from the G-P fitting were employed to compute the effective beam factor (EBF) for the chosen cement across various standard incident photon energies, specifically within the spectrum of 0.015–10 MeV, extending to 40 mean free paths, as delineated by the subsequent equations:

$$B(E,X) = 1 + ((b-1)/(K-1))(K\,\hat{}\,x\text{-}1)\ for\ K \neq 1$$
$$B(E,X) = 1 + (b\text{-}1)X\ for\ K = 1 \tag{8}$$

The function K (E, x) which represents the photon dose multiplication factor is rather a complicated tangent hyperbolic function and is given by:[42]

Table 1: Chemical compounds of the samples

Materials	Density (g/cm^3)	Mole fraction of elements (Fi.)												
		C	O	Al	Mg	Si	Ca	Na	Fe	Zn	Zr	S	W	Tl
Bricks	1.92	-	0.6327	0.0497	0.0053	0.2318	0.0615	-	0.019	-	-	-	-	-
Concrete	2.26	-	0.6422	0.0286	0.0026	0.2751	0.0427	0.0045	0.0041	-	-	-	-	-
Spot1	1.41	0.325	0.5002	-	-	0.0734	0.1014	-	-	-	-	-	-	-
Spot2	1.42	0.372	0.4658	-	-	0.0699	0.0924	-	-	-	-	-	-	-
Cement-plaster	1.52	-	0.6626	0.0320	0.0009	0.2254	0.0598	0.0009	0.0185	-	-	-	-	-
Cement composites	8.025	0.0129	0.5399	0.0251	0.0043	0.0056	0.0506	-	0.02608	0.0023	0.0012	0.0026	0.0129	0.0819

$$K(E,X) = CX^{a} + d\frac{tanh\left(\frac{X}{X_K} - 2\right) - tanh(-2)}{1 - tanh(-2)} \quad \text{for } x \leq 40mfp \qquad (9)$$

where x is the penetration depth in mean free path (mfp), E is the energy of the incident photon, K is the photon dose multiplicative factor and represent the spectrum shape change, and (b, c, a, X_k, d) are the calculated G-P fitting parameters in the previous step.

The parameter known as Σ_R, also known as the elimination cross-section, is defined as the probability of a neutron being moderated or removed from a set of energetic neutrons that have not yet interacted. The calculation of the Σ_R value for a composite material that consists of multiple elements is conducted through a specific process, which is outlined in detail in reference,[43] where various factors and properties of the constituent elements must be taken into account to arrive at an accurate representation of this parameter.

$$\Sigma_R / \rho = \sum_i W_i \left(\Sigma_R / \rho\right) \qquad (10)$$

where W_i partial density of ith constituent, Σ_j/ρ neutron mass attenuation coefficient of ith constituent for a specific interaction (j).

Monte Carlo simulation geant4

Geant4 is an object-oriented simulation toolbox that is widely used in many fields, including nuclear physics, medical physics. The importance and validity of Geant4 simulation are given in.[44] To investigate radiation shielding effects, the energy levels should cover well the energy spectrum of medical applications. The energy range relevant to diagnostic medical procedures is typically from 0.015 MeV to 0.5 MeV, whereas the energy range associated with therapeutic medical applications is considerably wider, encompassing values ranging from about 0.5 MeV to 10 MeV and thus highlights a remarkable spectrum in energy. To clarify the differences in the nature and thickness of shielding materials used in different energy spectrums, the energy spectrum is considered in the range of minimum 0.015 MeV to a maximum 10 MeV.[45] Within the context of the simulations conducted, the material was conceptualized as a cubic structure, with the dimensions of said cube meticulously measured at 10 cm × 10 cm × 1 cm along the respective x, y, and z coordinates. The representation of these can be visually appreciated in Figure 1. In Figure 1, the green lines that are prominently displayed within the confines of the cube serve as traces, indicating the trajectories of the gamma rays as they traverse through the material. The phenomenon of photon attenuation is intricately determined by simulating all conceivable physical processes that can occur for photons, which encompass mechanisms such as photoelectric effects, Compton scattering, Rayleigh scattering, and pair production, in addition to bremsstrahlung, ionization, and the annihilation of positrons and electrons. Each of these processes is meticulously modeled utilizing the physics models

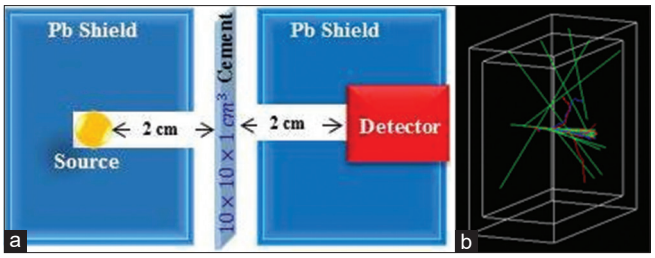

Figure 1: (a) setup of simulation. (b) Schematic of the configuration of shielding in Geant4 tool

that are specifically designed for electromagnetic interactions, which are integrated. These comprehensive physics models are predicated upon an electromagnetic package that utilizes evaluated data libraries, which are instrumental in providing the requisite data necessary for calculating cross-sections during the modeling of photon and electron interactions with matter.[46,47] In an effort to enhance the precision and reliability of the simulation outcomes, it is noteworthy that each simulation was conducted with a substantial sample size of 1 million gamma photons, employing option 4 of the electromagnetic physics framework. Finally, the methodology for calculating the generation factors utilized in these simulations can be readily accessed and comprehended in other scholarly sources, as indicated in reference.[42]

Phy-X program

The Phy-X/PSD software is employed for the computation of various shielding parameters across a spectrum of energy values. To facilitate these calculations, it is essential to provide the chemical composition of the material (expressed in moles or weight fraction) along with its density. The evaluation of shielding parameters is feasible within the photon energy range of 0.015–15 MeV. This software can proficiently and promptly compute eighteen distinct protection parameters. Designated photon energy values (ranging from 15 to 0.015 MeV) are incorporated as options within the Phy-X/PSD software, as they align with the energies emitted by radioactive isotopes (^{241}Am, ^{55}Fe, ^{133}Ba, ^{60}Co, ^{109}Cd, ^{132}E, ^{131}I, and ^{137}Cs) that may be utilized in medical, industrial, and nuclear settings where personnel are present.[48]

Results and Discussions

The values corresponding to the mass reduction coefficient, denoted as (μ_m), for the samples under investigation were meticulously calculated within the specified energy range that spans from 0.015 MeV to 10 MeV, utilizing the advanced Geant 4 simulation tool, which is renowned for its accuracy in simulating particle interactions. Furthermore, to ensure the robustness and reliability of the data that was derived from the simulation, pertinent information was extracted from the Phy-X database, thereby serving as a comparative benchmark to validate the findings obtained through the computational methods. It is imperative to acknowledge that the Phy-X code is fundamentally limited in its capabilities, as it is solely

designed to compute material attenuation based on theoretical principles, and it does not possess the functionality to derive the material attenuation coefficient utilizing the Monte Carlo transfer methodology. The percentage deviation, which reflects the discrepancies between the results produced by the Geant4 Monte Carlo simulation tool and those retrieved from the Phy-X database for the compounds that were examined, was observed to be approximately within the narrow range of 0.1% to 1%, thereby indicating a high degree of correlation between the two datasets. Such results compellingly demonstrate that the simulated μ_m values generated by the Geant4 simulation tool for the respective samples are remarkably congruent with the theoretical data provided by the Phy-X database, thus reinforcing the credibility of the simulation approach employed. Moreover, the comprehensive analysis encapsulated in Table 2 distinctly illustrates that the cement-based composite material exhibits the most significant damping coefficient when compared to the other materials assessed in this study. This finding underscores the exceptional properties of the cement-based composite, making it a subject of considerable interest for further research and application in fields requiring effective damping materials.

In Figure 2, we plotted the linear attenuation coefficient (LAC) for samples in the energy range of 0.015–10 energies. The LAC value for cement composite is higher than other samples, which shows the importance of adding elements with higher atomic numbers in improving the damping performance of a shield. Since zinc, iron, Tungsten, and Thallium are generally known to have high atomic numbers, we may predict that the cement composite contains more electrons and because the photon interacts with the electron cloud, it interacts with more orbital electrons. As a result, increasing the elements with higher atomic numbers can significantly improve the gamma-ray attenuation capabilities. Another important observation in Figure 2 is the relationship between LAC and energy. LAC is high for all samples at 0.1 MeV,

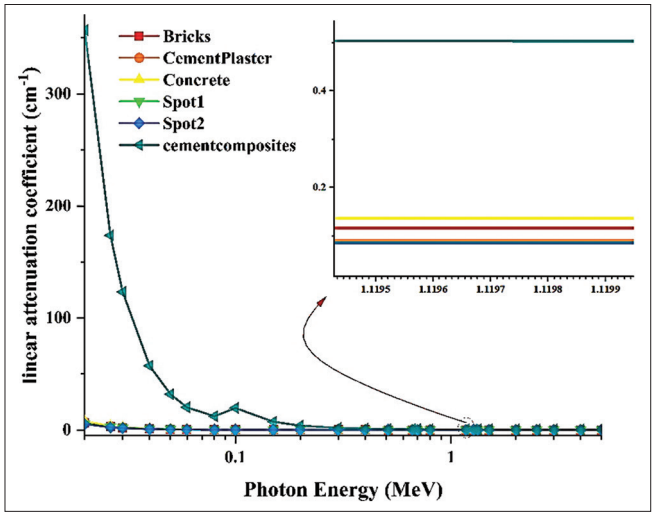

Figure 2: Linear attenuation coefficient (cm^{-1}) as energy photon in the samples

whereas it is small for other energies. At 0.1 MeV, the main contribution leading to these significant LAC values above these samples is made by the photoelectric effect. Furthermore, within the graphical representation, one can observe a pronounced peak that is indicative of the photoelectric edge specifically associated with the element tungsten, which plays a crucial role in understanding its interaction properties with electromagnetic radiation. Finally, with increasing energy and overcoming the Compton interaction, the linear attenuation coefficient decreases. The mass attenuation coefficient (MAC) diagram illustrates a variety of distinct mechanisms through which photons interact with matter across different energy regions, revealing nuanced insights into their behavior and characteristics. In the lower photon energy region, typically characterized by values that do not exceed 0.015 MeV, there is a pronounced reduction in the mass attenuation coefficient, which reflects how effectively the shielding medium can absorb incoming photons. Within this particular energy range, the photoelectric effect emerges as the predominant attenuation process; as a result, the shielding medium effectively absorbs a substantial proportion of the incident photons, leading to the observation of the highest mass attenuation coefficient values in this specific area of the spectrum. Transitioning to the energy region that spans from approximately 0.4 MeV to 2 MeV, it becomes evident that Compton scattering takes precedence as the primary interaction mechanism between photons and matter. During the process of Compton scattering, photons experience a loss of energy, undergo a change in direction, and subsequently scatter within the shielding material, a series of events that significantly contribute to the overall attenuation of radiation. This phenomenon results in a notable reduction in the capacity of high-energy photons to penetrate through the shielding materials employed. However, it is worth noting that the influence exerted by the chemical composition of the protective material on the process of Compton scattering remains relatively minimal. Consequently, it can be observed that all samples exhibit comparable mass attenuation coefficient values within this particular energy region, indicating a level of uniformity in their interaction behaviors. In energy ranges that exceed 1.02 MeV, photons attain sufficient energy levels that enable them to undergo a transformation into electron-positron pairs within the shielding material, a crucial phenomenon referred to as pair production. The occurrence of pair production events becomes increasingly significant as energy levels rise, particularly at energies that surpass 1.022 MeV. As depicted in Figure 3, it is evident that the mass attenuation coefficient values of the various samples exhibit a trend of increase with the incorporation of heavier elements, a relationship primarily attributable to the intricate connection between pair production events and the atomic number of the constituent elements present in the shielding material [Figure 3].

In the subsequent phase of our comprehensive investigation into the properties of materials, we meticulously analyzed the gamma-ray absorption characteristics exhibited by the

Table 2: Mass attenuation coefficients in terms of photon energy for samples

Energy (MeV)	Bricks			Cement plaster			Concrete		
	Geant4	Phy-x	±RD%	Geant4	Phy-x	±RD%	Geant4	Phy-x	±RD%
0.015	7.2593	7.2560	0.0455	10.6812	10.6952	0.1306	8.1351	8.1353	0.0027
0.02	3.1944	3.1839	0.3286	4.7548	4.7257	0.6116	3.5917	3.5765	0.4220
0.03	1.0735	1.0675	0.5546	1.5603	1.5504	0.6328	1.1968	1.1899	0.5721
0.04	0.5502	0.5484	0.3368	0.7557	0.7567	0.1335	0.6022	0.6011	0.1874
0.05	0.3622	0.3611	0.2959	0.4676	0.4687	0.2384	0.3889	0.3883	0.1421
0.0595	0.2799	0.2761	1.3862	0.3438	0.3386	1.5140	0.2961	0.2919	1.4256
0.08	0.2035	0.2038	0.1463	0.2297	0.2301	0.1755	0.2102	0.2105	0.1547
0.1	0.1729	0.1736	0.4036	0.1865	0.1870	0.2687	0.1764	0.1770	0.3697
0.15	0.1406	0.1416	0.7545	0.1444	0.1454	0.6897	0.1416	0.1426	0.7385
0.2	0.1250	0.1260	0.7983	0.1265	0.1274	0.7831	0.1254	0.1264	0.7944
0.3	0.1095	0.1076	1.6951	0.1074	0.1078	0.3639	0.1073	0.1077	0.3636
0.4	0.0960	0.0959	0.1067	0.0959	0.0958	0.1066	0.0960	0.0959	0.1066
0.511	0.0869	0.0873	0.5001	0.0867	0.0872	0.5046	0.0869	0.0873	0.5013
0.6617	0.0777	0.0807	3.7743	0.0775	0.0805	3.7923	0.0777	0.0806	3.7788
0.8	0.0713	0.0708	0.7105	0.0711	0.0705	0.7199	0.0712	0.0707	0.7129
1.5	0.0519	0.0518	0.3152	0.0518	0.0516	0.3309	0.0519	0.0518	0.3191
2	0.0446	0.0447	0.0957	0.0445	0.0446	0.0764	0.0446	0.0446	0.0907
3	0.0362	0.0364	0.4436	0.0362	0.0364	0.4295	0.0362	0.0364	0.4401
4	0.0316	0.0317	0.5653	0.0317	0.0319	0.5496	0.0316	0.0318	0.5614
5	0.0286	0.0288	0.5420	0.0289	0.0290	0.5282	0.0287	0.0289	0.5382
6	0.0267	0.0268	0.5226	0.0270	0.0271	0.5157	0.0267	0.0269	0.5209
8	0.0242	0.0243	0.4419	0.0246	0.0248	0.4474	0.0243	0.0245	0.4431
10	0.0228	0.0229	0.3935	0.0234	0.0235	0.4115	0.0230	0.0231	0.3980
15	0.0213	0.0213	0.1923	0.0220	0.0221	0.2314	0.0215	0.0215	0.2026
Energy (MeV)	**Spot1**			**Spot2**			**Cement composites**		
	Geant4	Phy-x	±RD%	Geant4	Phy-x	±RD%	Geant4	Phy-x	±RD%
0.015	8.8801	8.8863	0.0697	8.4025	8.4081	0.0661	81.7597	82.2592	0.6110
0.02	3.9652	3.9335	0.7980	3.7559	3.7262	0.7893	43.2458	43.2609	0.0350
0.03	1.3135	1.3068	0.5083	1.2505	1.2442	0.5015	14.9285	14.8649	0.4263
0.04	0.6497	0.6524	0.4206	0.6234	0.6259	0.4017	6.9572	6.9596	0.0347
0.05	0.4138	0.4151	0.3056	0.4003	0.4015	0.2781	3.8765	3.8833	0.1745
0.0595	0.3120	0.3075	1.4331	0.3039	0.2996	1.4096	2.4629	2.4317	1.2661
0.08	0.2170	0.2172	0.0788	0.2137	0.2139	0.0691	1.4859	1.5054	1.3105
0.1	0.1802	0.1806	0.1805	0.1785	0.1788	0.1838	2.3807	2.3698	0.4559
0.15	0.1429	0.1438	0.6865	0.1423	0.1433	0.6878	0.8954	0.8981	0.3003
0.2	0.1261	0.1271	0.7686	0.1259	0.1268	0.7662	0.4764	0.4752	0.2670
0.3	0.1077	0.1081	0.3524	0.1076	0.1080	0.3499	0.2259	0.2237	0.9804
0.4	0.0963	0.0962	0.1096	0.0962	0.0961	0.1100	0.1483	0.1481	0.0991
0.511	0.0871	0.0876	0.5056	0.0871	0.0875	0.5052	0.1127	0.1148	1.8429
0.6617	0.0779	0.0809	3.7822	0.0779	0.0808	3.7802	0.0891	0.0963	8.1156
0.8	0.0714	0.0709	0.7180	0.0714	0.0709	0.7170	0.0768	0.0762	0.8555
1.5	0.0520	0.0519	0.3091	0.0520	0.0519	0.3046	0.0509	0.0508	0.3232
2	0.0447	0.0447	0.0823	0.0447	0.0447	0.0844	0.0444	0.0444	0.0409
3	0.0362	0.0364	0.4439	0.0362	0.0364	0.4461	0.0385	0.0386	0.3325
4	0.0315	0.0317	0.5600	0.0315	0.0316	0.5623	0.0362	0.0362	0.1946
5	0.0286	0.0287	0.5405	0.0285	0.0286	0.5442	0.0353	0.0352	0.0677
6	0.0266	0.0267	0.5330	0.0264	0.0266	0.5351	0.0350	0.0349	0.2887
8	0.0241	0.0242	0.4535	0.0239	0.0240	0.4545	0.0354	0.0352	0.5388
10	0.0226	0.0227	0.4085	0.0225	0.0226	0.4068	0.0362	0.0360	0.4913
15	0.0210	0.0210	0.2194	0.0208	0.0208	0.2153	0.0387	0.0387	0.0302

RD: Relative deviation

samples under scrutiny, and in doing so, we determined the HVL values which are indicative of the materials' interactions with gamma radiation at various energy levels. It is critical to understand that the fundamental behavior of gamma-ray

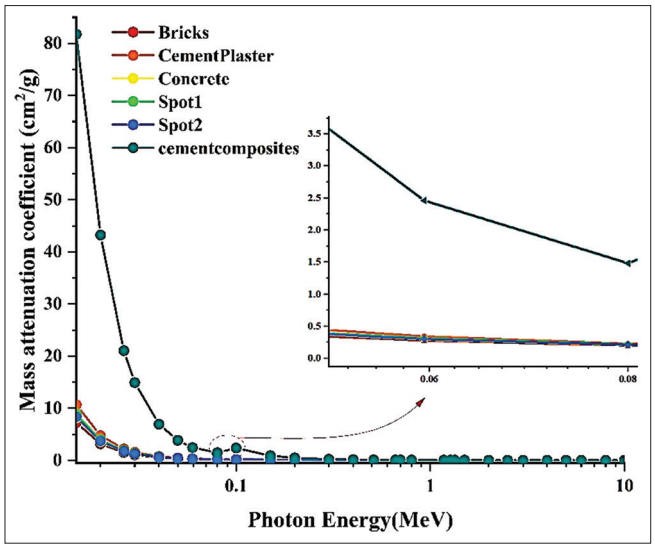

Figure 3: Mass attenuation coefficient (cm^2/g) as energy photon for samples

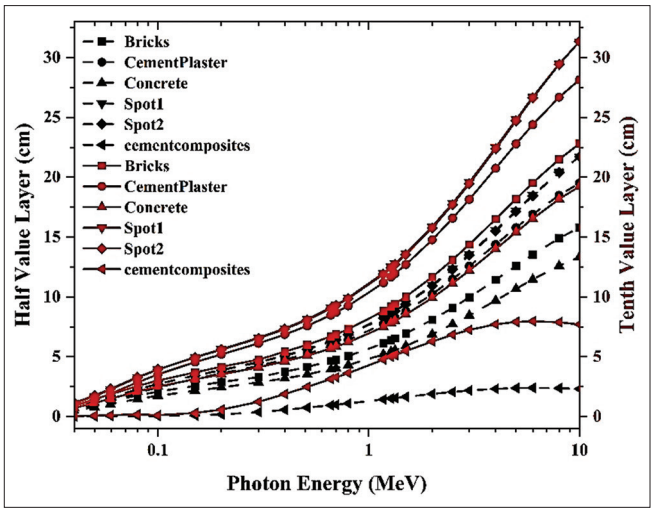

Figure 4: The half-value layer and tenth-value layer as energy photon in the samples

attenuation within a material, particularly at lower thicknesses, is predominantly governed by the measurement of the low HVL that is observed for a specific energy value, which serves as a crucial parameter in radiation shielding studies. As illustrated in Figure 4, there are discernible changes in the HVL values that correspond to the progressive increase in gamma-ray energy, which can be interpreted as an essential finding in materials science. Upon careful examination of the data presented in Figure 4, it becomes evident that the recorded values for the HVL indicate that low-energy gamma rays exhibit the lowest HVL values, reflecting their limited penetration capabilities. Conversely, there is a notable increase in the HVL values as the energy of the gamma rays rises, which can be attributed to the inherent physical properties of the materials and the energy interactions involved. This phenomenon can be primarily linked to the restricted capacity of low-energy gamma rays to effectively penetrate through the various materials being investigated, highlighting the complexities of radiation interactions. The observed trends in both the HVL and TVL curves align with the established processes of background photon interactions, which are fundamental to our understanding of radiation physics. It is noteworthy that low-energy photons tend to rapidly dissipate their energy at relatively shallow depths within the examined samples, which corroborates the behavior we anticipated based on theoretical models. However, it is also important to recognize that the HVL and TVL values reach their peak at the juncture where Compton scattering becomes the dominant interaction mechanism, further elucidating the complexities of photon behavior in materials. As the energy of the photons continues to increase, a coupling effect is produced, which ultimately leads to a decrease in both the HVL and TVL values, signifying a shift in the radiation interaction dynamics. Moreover, the incorporation of heavy elements into the composite materials significantly influences these HVL and TVL values, resulting in a gradual reduction in the required thickness for effective shielding in the samples being analyzed. An essential consideration in our findings is that our proposed composite material, due to its considerable density and atomic weight, necessitates only half the thickness of the shielding material when compared to other samples to achieve a level of radiation protection that is equivalent, demonstrating its potential efficacy in practical applications. The mass–energy transfer coefficients serve as a quantitative representation of the average fractional energy of incident photons that is converted into the kinetic energy of charged particles, which occurs as a direct consequence of the complex interactions between photons and the atomic constituents of the material under consideration. Various phenomena, including incoherent scattering, the atomic photoelectric effect, and the generation of positron-electron pairs, exemplify these characteristics and contribute significantly to our understanding of photon interactions. The determination of these coefficients is accomplished by utilizing the cross-sectional area associated with these specific interactions as well as the ratio derived from the kinetic energy of the charged particles, which is in turn related to the energy of the incident photons as a result of each respective interaction taking place. In addition, the various events that gamma rays undergo subsequent to their interaction with matter are crucial elements that must be taken into account when calculating the coefficients of energy absorption and distribution. In the illustration presented in Figure 5, it becomes abundantly clear that the quantity of energy that is transferred by the photon as it traverses through the protective shield composed of composite cement is significantly lower when compared to other sample materials that have been evaluated in this context. This particular scenario unequivocally demonstrates that a reduced fraction of the photon energy is converted into kinetic energy for the electrons, especially in the energy range where the Compton scattering interaction prevails, or alternatively, where the electrons experience scattering at notably smaller angular

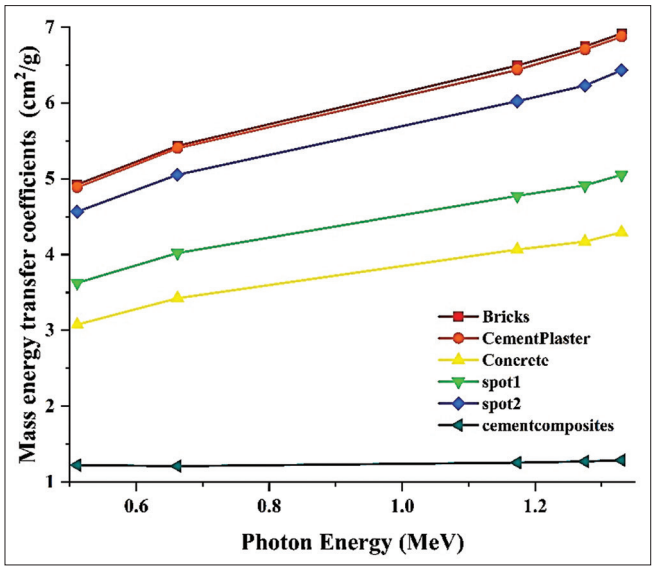

Figure 5: The mass-energy transferred coefficients as energy photon in the samples

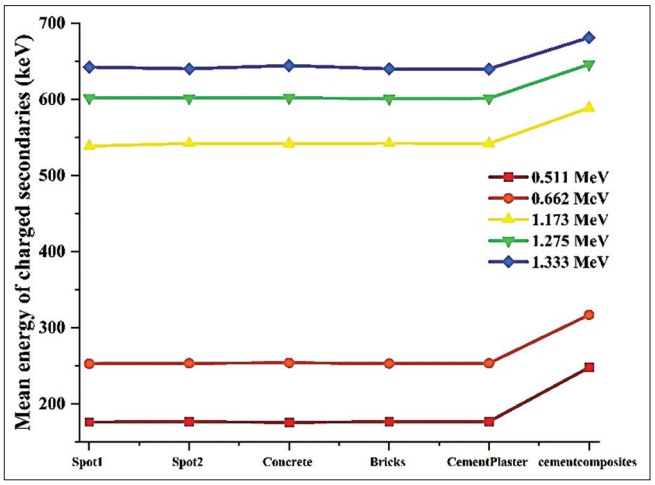

Figure 6: The mean energy of charged secondaries as energy photon in the samples

deviations. Ultimately, when making a comparative analysis of absorption versus attenuation, it is evident that the absorption phenomenon associated with composite cement is markedly higher than that observed in the other materials that have been subjected to examination. The phenomenon known as secondary emission can be comprehensively defined as a process, in which primary incident particles, possessing a level of energy that is deemed sufficient, interact with a surface or traverse through a specific material, thereby instigating the ejection of secondary particles from that surface or material. This concept is frequently associated with the emission of electrons, particularly in scenarios where charged particles, such as electrons or ions, are utilized within a shielding context, leading to the subsequent release of additional charged particles. Figure 6 illustrates the intricate dynamics of energy transfer, demonstrating the extent to which a photon imparts energy to electrons while simultaneously experiencing a reduction in its own energy as it traverses through the material in question. Within the spectrum of the selected energy levels, it is noteworthy that the average energy of the secondary particles generated is significantly elevated in comparison to other samples analyzed, which serves as a compelling indicator of the superior efficacy exhibited by composite cement in its capacity to effectively absorb gamma rays. This observation not only underscores the material's performance but also highlights the potential implications for its application in fields requiring enhanced radiation shielding and energy absorption capabilities.

The effective atomic number (Z_{eff}) is a parameter used to describe the attenuation of a beam of X-rays or gamma rays as they pass through a material. It is a weighted average of the atomic numbers of the elements in the material, taking into account their relative abundances and the energies of the incident photons. The effective atomic number is a useful parameter for describing the attenuation of X-rays or gamma rays in complex materials, such as biological tissues, which are composed of a mixture of elements. It provides a single value that can be used to compare the attenuation properties of different materials, even if their compositions are different. There are several different methods for calculating the effective atomic number of a material, but the most commonly used method is the mixture rule. The mixture rule assumes that the attenuation of X-rays or gamma rays in a material is due to a combination of photoelectric absorption and Compton scattering and that the contribution of each element to the attenuation can be approximated by its mass attenuation coefficient. Any compound that has heavier elements will have a better atomic number, which has a direct relationship with density. As it is known, compounds that have higher density have a higher effective atomic number than others and this is clearly evident for composite cement [Figure 7].

The effective electron density (N_{eff}) is a parameter used to describe the attenuation of a beam of charged particles, such as electrons or beta particles, as they pass through a material. It is defined as the number of electrons per unit volume that would produce the same amount of attenuation as the material itself. The effective electron density takes into account the density and composition of the material, as well as the energies and angular distributions of the incident particles. It is a useful parameter for describing the stopping power of a material for charged particles and is commonly used in radiation therapy and in the design of radiation shielding. The effective electron density can be used to calculate the stopping power of a material for charged particles, using the Bethe–Bloch formula or other similar equations. It can also be used to optimize the design of radiation shielding, by selecting materials with high effective electron densities and low atomic numbers. Figure 8 shows that at low energies, it has a better performance to stop charged particles, and at energies of 0.05 MeV to 0.4 MeV, composite cement can stop charged particles better. After the energy of 0.4 MeV, the electron density decreases drastically,

which is due to the dominant Compton interactions in this region. With the increase of 2 MeV energy and the dominance of pair production, the electron density increases. This is contrary to other samples, the reason for which is the presence of elements with higher atomic numbers in composite cement.

It can be seen that the EBF values for all samples increase to a maximum value at intermediate energies and then start to decrease. In the low-energy region (E < 0.2 MeV), the photoelectric effect of the photon interaction process is dominant, and its cross-section changes with energy in the form of $E^{3.5}$. Due to the dominance of this process, the maximum number of photons are absorbed by the samples. Hence, it leads to a decrease in the EBF value in the lower energy region. Similarly, in the higher energy region (E > 1.022 MeV), another photon absorption process, which is pair production, is the dominant process whose cross-section changes inversely with energy as E^2. However, in the intermediate energy region (0.2< E < 1 MeV), Compton scattering is a dominant photon interaction process, which only contributes to the destruction of photon energy due to scattering and cannot completely remove the photon. Therefore, in this energy region, the lifetime of the photon is longer, and hence the probability of the photon escaping from the shield is also higher. This process leads to an increase in EBF value. According to equations 8 and 9, it was also observed that the EBF values for the largest penetration depth of 40 mfp became too high due to multiple scattering events for large penetration depths. On the other hand, when charged particles pass through a material, they experience multiple collisions with atoms or electrons in the material. These collisions cause the loss of energy and scattering of particles, which leads to the expansion of their energy distribution. EBF quantifies the emission of this energy and is defined as the ratio of the standard deviation of the energy to the average energy (E) of the particles after passing through the material. The EBF also increases with the atomic number and density of the material, as these factors increase the frequency of scattering events. It is also relevant for particle transport simulations, such as Monte Carlo simulations, which require accurate modeling of energy dissipation and particle dispersion as they pass through materials. The EBF value is much lower for cement composite and gypsum concrete, which shows that even in the higher mean free path, it can better prevent particle dispersion and improve the protection performance in Figure 9 (a-f).

Figure 10 shows the fast neutron attenuation coefficients (Σ_R) of the examined samples. The addition of carbon and thallium increases the neutron shielding capabilities of cement composite and leads to higher Σ_R. Specifically, the cement composite shows the highest Σ_R value of 0.134, whereas the other samples have the lowest value of 0.07. This capability may make cement composite a suitable option for protection against gamma and neutron radiation.

Table 3 shows the effective interactions in the thermal neutron cross-section. For spots 1 and 2, the inelastic interaction is

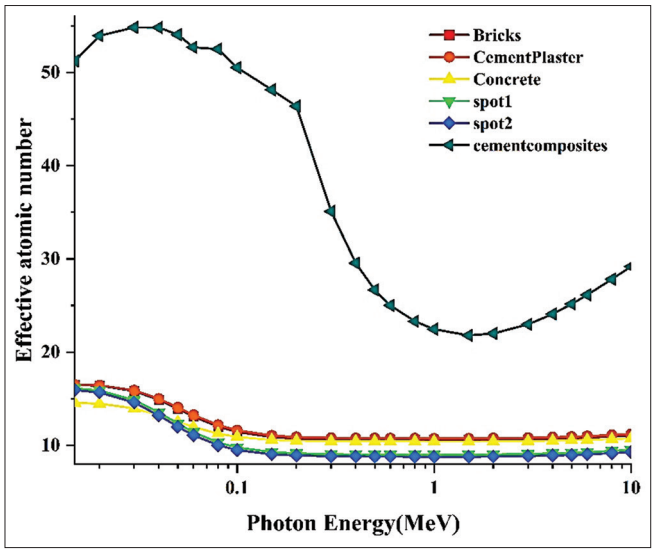

Figure 7: The effective atomic number, $Z_{eff\ as}$ energy photon in the samples

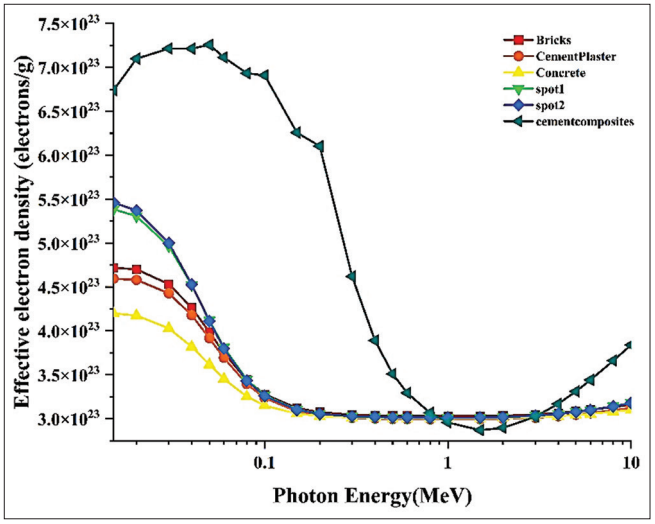

Figure 8: The effective electron density, N_{eff}, as energy photon in the samples

Table 3: Cross-section of thermal neutron interactions for samples

Interactions cross section (mm^2/g)	Material					
	Bricks	Cement plaster	Concrete	Spot1	Spot2	Cement composites
Neutron-elastic	8.8889	4.2687	8.7419	12.263	12.821	4.5533
Neutron-capture	0.31312	0.99976	0.35022	0.13401	0.13079	6.918
Neutron-inelastic	0.472×10^{-4}	424.41×10^{-2}	5.178×10^{-4}	-	-	149.79×10^{-4}
Total	8.8892	4.6941	8.7427	12.263	12.821	4.5752

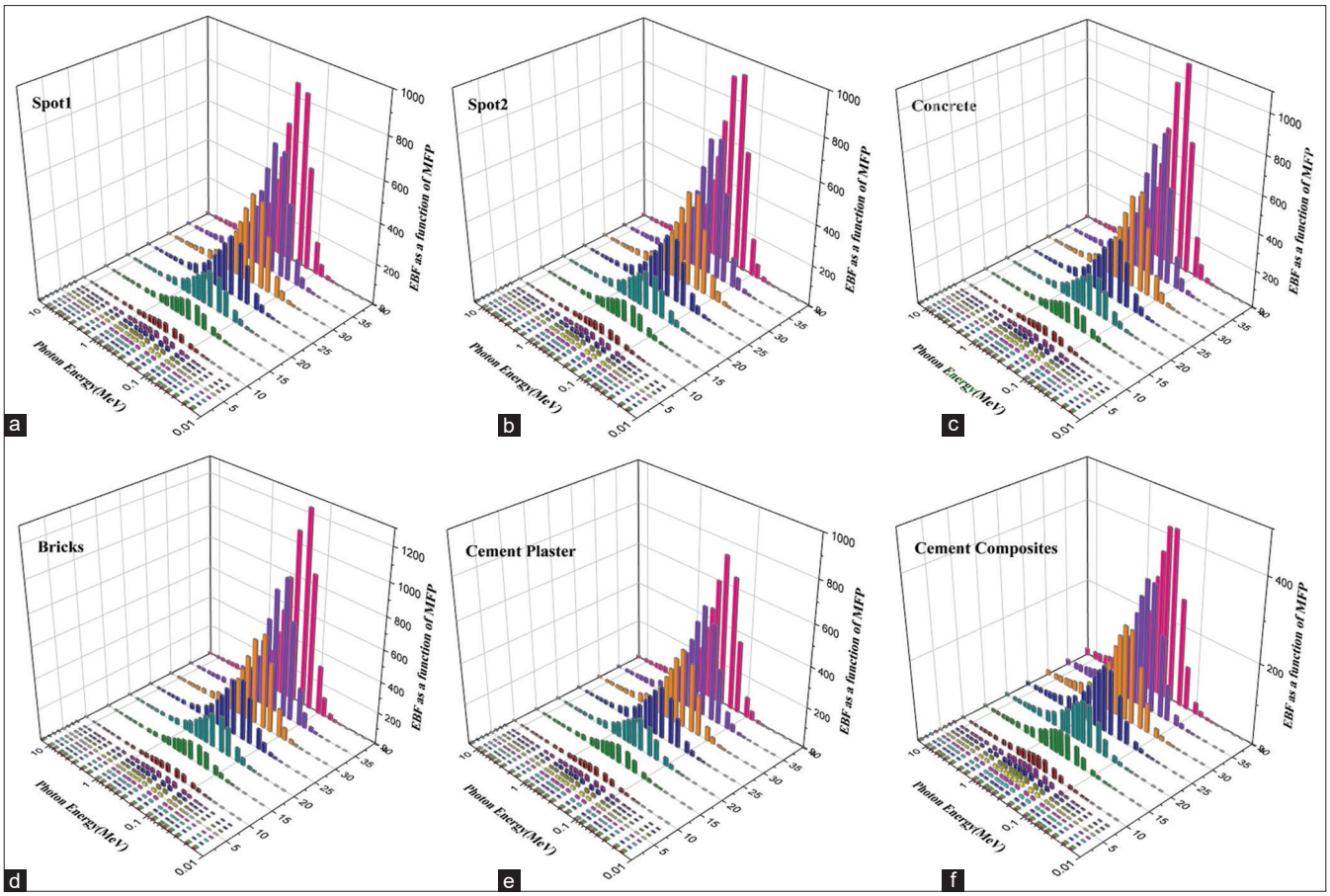

Figure 9: (a-f) Effective beam factor as a function of mean free path (MFP) in different energies

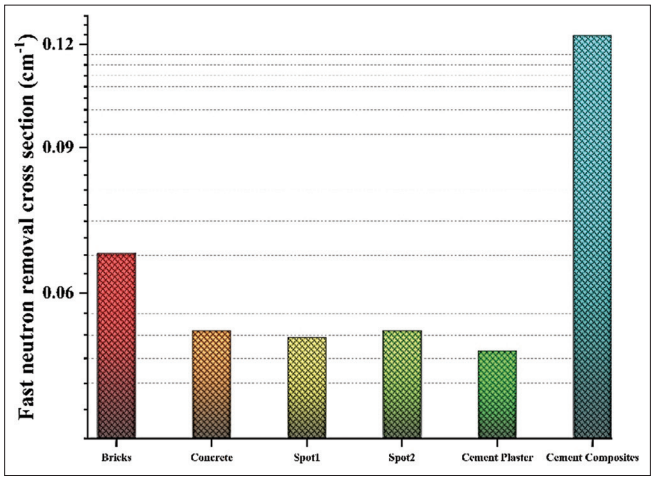

Figure 10: The fast neutrons removal cross section of in the samples

much less (of the order of 10^{-6}) than in other samples, and the reason for its smallness was ignored. As it is clear from the table, the absorption rate of thermal neutrons in composite cement is about 7 times that of other samples. Figure 11 shows the absorption rate of neutrons passing through a 1 mm to 1 cm sample. The decrease in the number of passing or reduced neutrons is clearly visible. Neutron attenuation is exponential in thickness and strongly depends on the macroscopic cross-section of neutron interactions. The neutron measurement results for different thicknesses for all samples are summarized in Figure 11. Finally, with the conclusion from Table 2 and Figure 10, these results were predictable and show the proper performance of cement composite against fast and thermal neutrons.

Conclusions

Current work investigates a cementitious composite modified with carbon, thallium, and tungsten elements for use in radiation shielding applications. Adding these elements increases the density of the composite, where the density of common concrete is between 2.35 and 2.22 g per cubic centimeter, this cement composite has a density of 8.025 g per cubic centimeter. The percentage deviation, which reflects the discrepancies between the results produced by the Geant4 Monte Carlo simulation tool and those retrieved from the Phy-x database for the compounds that were examined, was observed to be approximately within the narrow range of 0.1% to 1%, thereby indicating a high degree of correlation between the two datasets. The mass attenuation coefficient of cement composite is 81.75 cm^{-1} (at 0.015 MeV), which is increased 10 times compared to other samples. These features reduced the HVL from 23 cm to 2.5 cm (at 10 MeV). The addition of heavy elements to the sample increases their radiation

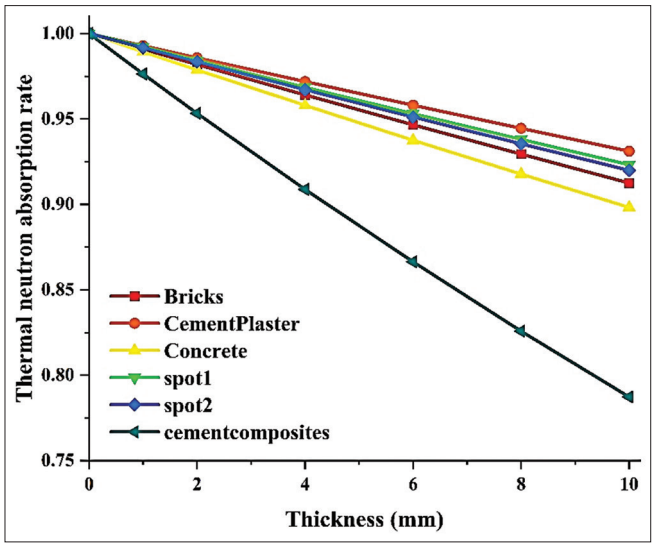

Figure 11: The thermal neutron absorption rate in the samples

shielding efficiency, where the radiation shielding efficiency for the developed cement composite increased by 87% at all energies, while the radiation shielding properties of the 33 cm thick cement composite were 7 cm and reaches 10 MeV. Therefore, a 7 cm thick wall made of concrete is enough to absorb more than 85% of the released photons with high energies up to 3 MeV. The net result shows that the developed concretes have suitable radiation shielding applications for use in the construction of medical and radiology centers and other radiation shielding applications.

Financial support and sponsorship

Nil.

Conflicts of interest

There are no conflicts of interest.

References

1. Nichols TL, Byrne T. Health effects and radiation biology. Encyclopedia of Nuclear Energy; 2021. p. 923-36.
2. Hanfi MY, Sayyed MI, Lacomme E, Akkurt I, Mahmoud KA. The influence of MgO on the radiation protection and mechanical properties of tellurite glasses. Nucl Eng Technol 2021;53:2000-10.
3. Tochaikul G, Mongkolsuk M, Kobutree P, Kawvised S, Pairodsantikul P, Wongsa P, *et al*. Properties of cement Portland composite prepared with Barium sulfate and Bismuth oxide for radiation shielding. Radiat Eff Defects Solids 2023;179:548-66. [doi: org/10.1080/10420150.2023.2294037].
4. Wang J, Zhao Y, Shi D, Xia Y, Liu M, Ma X, *et al*. Microstructure and radiation shielding properties of lead-fiber reinforced high-performance concrete. Ceram Int 2024;50:23656-67. [doi.org/10.1016/j.ceramint.2024.04.089].
5. Krishnasamy J. Chapter 11 - State-of-the-art review on the neutron and ionizing radiation shielding. Advanced Radiation Shielding Materials (Radiation and Radiological Protection); 2024. p. 273-88. [doi: org/10.1016/B978-0-323-95387-0.00004-2].
6. Sobczak J, Żyła G. Nano and microcomposites as gamma and X-ray ionizing radiation shielding materials — A review. Energy 2024;290:130210.
7. Olarinoye IO, Kolo MT, Shittu HO, Anumah AS. Estimation of indoor gamma radiation dose rate from concrete blocks constructed from tin mine tailings. J Build Eng 2023;66:105934.
8. Jain A, Agrawal V, Gupta R. Using serpentine in concrete: A literature review. Mater Today Proc 2023. [doi: 10.1016/j.matpr. 2023.03.138].
9. Zhang P, Sun X, Wang F, Wang J. Mechanical properties and durability of geopolymer recycled aggregate concrete: A review. Polymers (Basel) 2023;15:615.
10. Kanthe VN. Effect of superplasticizer on strength and durability of rice husk ash concrete. Iran J Energy Environ 2021;12:204-8.
11. Singh A, Kumar R, Mehta PK, Tripathi D. Effect of nitric acid on rice husk ash steel fiber reinforced concrete. Mater Today Proc 2020;27:995-1000.
12. Mansour MA, Ismail MH, Latif QB, Alshalif AF, Milad A, Bargi WA. Systematic review of the concrete durability incorporating recycled glass. Sustainability 2023;15:3568. [doi: org/10.3390/su15043568].
13. Hamada K, Nomura K. The over-valued yen and the low-pressure economy repressed productivity in Japan. Int J Econ Finance 2023;15:1.
14. Li T, Xin R, Wang D, Yuan L, Wu D, Wu X. Research progress on the applications of seashell adsorption behaviors in cement-based materials. Buildings 2023;13:1289.
15. Kanagaraj B, Anand N, Cashell KA, Andrushia AD. Post-fire behaviour of concrete containing nano-materials as a cement replacement material. Case Stud Construction Mater 2023;18:e02171.
16. Farid SA, Zaheer MM. Production of new generation and sustainable concrete using rice husk ash (RHA): A review. Mater Today Proc 2023. [doi: org/10.1016/j.matpr.2023.06.034].
17. Khan K, Ahmad W, Amin MN, Deifalla AF. Investigating the feasibility of using waste eggshells in cement-based materials for sustainable construction. J Mater Res Technol 2023;23:4059-74.
18. Günoğlu K, Akkurt I, Sayyed MI. Radiation shielding properties of some igneous rocks in isparta province at different gamma energies: Experimental and theoretical study. J Radiat Res Appl Sci 2024;17:100796.
19. Xiao Z, Xie S, Hu A, Chen Y, Wang M. Displacement control in irregular deep excavation adjacent to tunnel groups in structural soil: A case study of MJS cement-soil composite piles and grouting rectification. Case Stud Construction Mater 2024;20:e03085.
20. Mahmoud KA, Tashlykov OL, Wakil AF, Aassy IE. Aggregates grain size and press rate dependence of the shielding parameters for some concretes. Prog Nucl Energy 2020;118:103092.
21. Bantan RA, Sayyed MI, Mahmoud KA, Al-Hadeethi Y. Application of experimental measurements, Monte Carlo simulation and theoretical calculation to estimate the gamma ray shielding capacity of various natural rocks. Prog Nucl Energy 2020;126:103405.
22. Fan JL, Zhang F, Chen Q, Song HC, Zhong LY, Dai YX. A novel algorithm for evaluating cement azimuthal density based on perturbation theory in horizontal well. Pet Sci 2024;21:244-51. [doi: 10.1016/j.petsci. 2023.10.007].
23. Kanagaraj B, Anand N, Raj S, Lubloy E. Advancements and environmental considerations in portland cement-based radiation shielding concrete: Materials, properties, and applications in nuclear power plants–review. Clean Eng Technol 2024;19:100733.
24. Korkmaz AV, Hacıfazlıoğlu H, Akkurt İ. Radiation attenuation characteristics of meta-schist modified Portland cement: Comparative analysis with traditional cement. Case Stud Construction Mater 2024;20:e02737.
25. Rilwan U, Aliyu GM, Olukotun SF, Idris MM, Mundi AA, Bello S, *et al.* Recycling and characterization of bone incorporated with concrete for gamma-radiation shielding applications. Nucl Eng Technol 2024;56:2828-2834.[doi: 10.1016/j.net.2024.02.045].
26. Florez R, Giraldo Carlos HC, Restrepo-Arcila SM, Colorado HA. Valorization of spent Zn-C battery and construction and demolition waste (CDW): Fabrication and characterization of geopolymer composites for radiation shielding applications. Open Ceram 2024;18:100588.
27. Alomayrah N, Alrowaili ZA, Alalawi A, Al-Buriahi. Gamma and neutron attenuation of ASM geopolymers for radiation shielding applications: Theoretical study. J Radiat Res Appl Sci 2024;17:100876.
28. Mahmoud KG, Alqahtani MS, Tashlykov OL, Semenishchev VS, Hanfi MY. The influence of heavy metallic wastes on the physical properties and gamma-ray shielding performance of ordinary concrete:

Experimental evaluations. Radiat Phys Chem 2023;206:110793.
29. Ramadan M, El-Gamal SM, Wetwet MM, Hazem MM. Amelioration of antimicrobial, radiation shielding, thermal stability of Portland cement composites using hematite nanoparticles. Construction Build Mater 2024;421:135661.
30. Jahan MS, Hossain S, Sayeed MA, Das SC, Grammatikos S, Pingky SY, *et al*. Development of heavy mineral filler based FRP composites for (low energy) radiation shielding application. Radiation Effects and Defects in Solids, 2024;179:1132-52. [doi: org/10.1080/10420150.2024.2332195].
31. Al-Saleh WM, Elsafi M, Almutairi HM, Nabil IM, El-Nahal MA. A comprehensive study of the shielding ability from ionizing radiation of different mortars using iron filings and bismuth oxide. Sci Rep 2024;14:10014.
32. Alfryyan N, Alsaif NA, Al-Ghamdi H, Issa SA, Zakaly HM, El-Hamalawy AA, *et al.* Investigation of borate glasses reinforced with iron (III) oxide [Fe2O3]: Preparation, physical, UV–Vis properties and γ-ray attenuation efficacy. Optical Mater 2024;152:115424.
33. Babeer AM, Amin HY, Sayyed MI, Mahmoud AE, Abdo MA, Ellakwa TE, *et al.* Impact of mixed heavy metal cations (Ba and Bi) on the structure, optical and ionizing radiation shielding parameters of Bi2O3–BaO–Fe2O3–SrO–B2O3 glass matrix. Ceram Int 2024; 50:19245-58.
34. Abo-El-Enein SA, El-Hosiny FI, El-Gamal SMA, Amin MS, Ramadan M. Gamma radiation shielding, fire resistance and physicochemical characteristics of Portland cement pastes modified with synthesized Fe2O3 and ZnO nanoparticles. Constr Build Mater 2018;173:687-706.
35. Fudger SJ, Luckenbaugh TL, Hornbuckle BC, Darling KA. Mechanical properties of cemented tungsten carbide with nanocrystalline FeNiZr binder. Int J Refractory Metals Hard Mater. 2024;118:106465.
36. Evstegneeva NA, Kolesnikov SI, Timoshenko AN, Minnikova TV, Tsepina NI, Kazeev KS. Assessment of thallium ecotoxicity by biological properties of soils. Eurasian Soil Sci 2024;57:482-92.
37. Irshidat MR, Al-Nuaimi N. Industrial waste utilization of carbon dust in sustainable cementitious composites production. Materials (Basel) 2020;13:3295.
38. Singh GV, Subramaniam KV. Production and characterization of low-energy Portland composite cement from post-industrial waste. J Clean Prod 2019;239:118024.
39. Bahraq AA, Maslehuddin M, Al-Dulaijan SU. Macro- and micro-properties of engineered cementitious composites (ECCs) incorporating industrial waste materials: A review. Arab J Sci Eng 2020;45:7869-95.
40. Li X, Qin D, Hu Y, Ahmad W, Ahmad A, Aslam F, *et al*. A systematic review of waste materials in cement-based composites for construction applications. J Build Eng 2022;45:103447.
41. Alipoor M, Eshghi M. Shielding properties of iron-doped nano-hydroxides against gamma-rays. J Nucl Sci Eng Technol 2024;45:148-57. [doi: 10.24200/nst.2024.1643].
42. Sayyed MI, AlZaatreh MY, Matori KA, Sidek HA, Zaid MH. Comprehensive study on estimation of gamma-ray exposure buildup factors for smart polymers as a potent application in nuclear industries. Res Phys 2018;9:585-92.
43. Abdullah KH, Mahmod SA. Calculation the fast neutrons interaction parameters for several carbohydrates. Stallion J Multidiscip Assoc Res Stud 2024;3:56-62.
44. Park J, Teh FC, Tsang MB, Brown KW, Chajecki Z, Hong B, *et al.* neuSIM4: A comprehensive GEANT4 based neutron simulation code. Nucl InstrumMethods Phys Res A Accelerators Spectrometers Detectors Assoc Equipment 2024;1065:169475.
45. Turker NS, Özer AY, Çolak Ş, Kutlu B, Nohutçu R. ESR investigations of gamma irradiated medical devices. Appl Radiat Isot 2017;130:121-30.
46. Alipoor MR, Eshghi M. Nickel/multiwalled Carbon Nanotube Composites as Gamma-ray Shielding. NANO; 2024; 19. [doi: org/10.1142/S1793292024500279].
47. Eshghi M, Alipoor M. A comprehensive study of gamma-rays shielding features of binary compounds. Prog Phys Appl Mater 2024;4:59-67.
48. Mohammed MI, Yahia IS, Zahran HY. Radiation attenuation parameters of Ti3SiC2 MAX phase and their binary compounds using Phy-X/PSD software. Mater Sci Semicond Process 2024;169:107916.